New Miniaturized Dual-Mode Dual-Band Ring Resonator Bandpass Filter With Microwave C-Sections

Yi-Chyun Chiou, *Member, IEEE*, Cho-Yu Wu, and Jen-Tsai Kuo, *Senior Member, IEEE*

***Abstract*—A new miniaturized dual-mode dual-band ring resonator bandpass filter is implemented by a cascade of several microwave C-sections. Each C-section is used to substitute a transmission line section of designated electrical length. Through proper design of input/output coupling configuration, two transmission zeros can be created on both sides of each passband. Two circuits with four and six microwave C-sections are fabricated for confirmation. They occupy less than 30% of the area of a traditional ring resonator filter. Measured responses agree very well with the simulation.**

***Index Terms*—Bandpass filter (BPF), dual-band, dual-mode, microwave C-section, miniaturized.**

I. Introduction

RING resonator filters have been widely used in front-ends of microwave systems due to their compact size and easy design [1]–[3]. The circuit in [1] could be the first ring resonator bandpass filter (BPF) with two degenerate modes that are of essential importance for constituting the passband. The quasi-elliptic BPF in [2] is designed to have tunable transmission zeros with a constant bandwidth. In [3], a periodic stepped-impedance ring resonator is devised to develop a miniaturized dual-mode filter with a wide upper stopband. Notice that all these circuits involve BPFs with a single passband.

Recently, rapid development of modern wireless systems, such as GSM and WLAN, has created a need for dual-band RF devices. Several dual-mode dual-band BPFs have been published [4]–[8]. In [4], the stacked-loop structure consists of two dual-mode rings on different layers and each ring resonator controls one passband. Based on a similar idea, an alternative dual-band filter with a coplanar waveguide (CPW) feed line is carried out in [5]. In [6], a loop resonator is proposed for a planar dual-band filter. The feed lines are placed between two resonators to offer sufficient coupling for both passbands. The dual-band filter in [7] is designed in a multilayer structure consisting of dual-mode resonators in a reflector cavity. It is noted that each selected passband in [4]–[7] is mainly controlled by a resonator. The dual-mode dual-band filter in [8] is contrived with a single stepped-impedance ring resonator.

In this letter, a dual-mode dual-band BPF is implemented with microwave-C sections, which have nonlinear phase shift property in frequency [9] and are suitable for development of dual-band devices [10]. Here, each microwave C-section is used to substitute a $\lambda/4$- or $\lambda/6$-section of a traditional ring. Analysis will be conducted and design curves plotted for facilitating the circuit realization. Emphasis is also put on the input/output configuration for creating transmission zeros on both sides of each passband. Two circuits are simulated, fabricated and measured for confirmation.

II. Formulation

Fig. 1 shows the elementary two-port for constructing the dual-mode dual-band filter. It consists of two transmission line sections of length θ_1 and characteristic impedances Z_1 with a microwave C-section of electric length θ_c in between. In our approach, a uniform ring is treated as a cascade of N identical sections and each of them will be implemented by the network in Fig. 1. Then, let the two designated frequencies be f_1 and $f_2 = nf_1$, and the characteristic impedance of the ring peripheral be Z_u. For simplicity, $Z_1 = Z_u = \sqrt{Z_{oe}Z_{oo}}$ is chosen, where Z_{oe} and Z_{oo} are the even- and odd-mode characteristic impedances of the coupled-line. By enforcing the $ABCD$ matrix of the two-port to be equal to those of a uniform section of $\theta_u = 2\pi/N$ and $2\theta_u$ at f_1 and f_2, respectively, the following four equations can be readily obtained:

$$F(\theta_c)\cos 2\theta_1 + 2Z_1 \sin 2\theta_1 = E(\theta_c)\cos\theta_u \quad (1a)$$

$$F(\theta_c)\sin 2\theta_1 - 2Z_1 \cos 2\theta_1 = E(\theta_c)\sin\theta_u \quad (1b)$$

$$F(n\theta_c)\cos 2n\theta_1 + 2Z_1 \sin 2n\theta_1 = E(n\theta_c)\cos 2\theta_u \quad (1c)$$

$$F(n\theta_c)\sin 2n\theta_1 - 2Z_1 \cos 2n\theta_1 = E(n\theta_c)\sin 2\theta_u \quad (1d)$$

where

$$E(\varphi) = -Z_{oe}\cot\varphi - Z_{oo}\tan\varphi \quad (2a)$$

$$F(\varphi) = -Z_{oe}\cot\varphi + Z_{oo}\tan\varphi. \quad (2b)$$

Based on (1) and (2), Fig. 2 plots z_{oe}, z_{oo} and θ_c as functions of n for $\theta_u = 60^\circ$ with $\theta_1 = 14^\circ$ and $\theta_u = 90^\circ$ with $\theta_1 = 24^\circ$. Here, $Z_1 = 85\,\Omega$ is chosen and z_{oe} and z_{oo} are, respectively, Z_{oe} and Z_{oo} normalized with respect to $Z_o = 50\ \Omega$, the reference port impedance. Such a high Z_1 is chosen since narrow lines are capable of providing sufficient coupling to our dual-band design. In Fig. 2, z_{oe} and z_{oo} gradually decrease and increase,

Manuscript received August 06, 2009; revised November 17, 2009. First published January 19, 2010; current version published February 10, 2010. This work was supported in part by the MoE ATU program and by the National Science Council of Taiwan under Grants NSC 98-2221-E-009-032-MY2 and NSC 98-2218-E-009-011.

The authors are with the Institute of Communication Engineering, National Chiao Tung University, Hsinchu 300, Taiwan (e-mail: jtkuo@mail.nctu.edu.tw).

Color versions of one or more of the figures in this letter are available online at http://ieeexplore.ieee.org.

Digital Object Identifier 10.1109/LMWC.2009.2038432

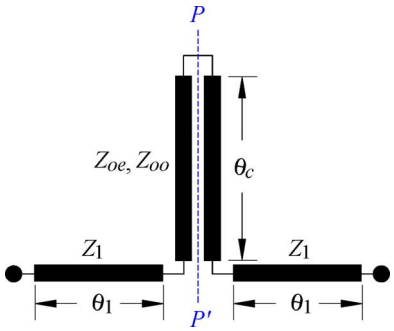

Fig. 1. Microwave-C section for substituting a transmission line section.

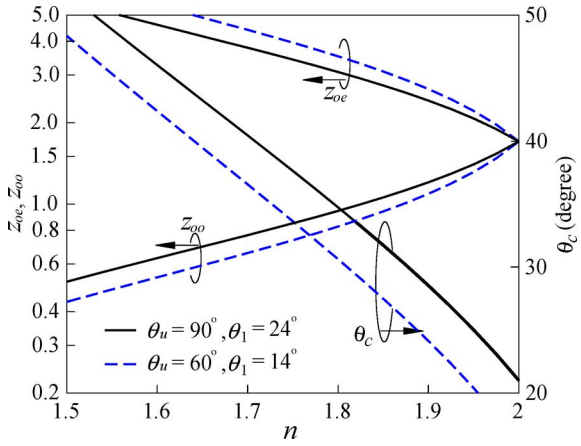

Fig. 2. z_{oe}, z_{oo} and θ_c as functions of n.

respectively, when n is increased from 1.5 to 2. It is noted that when $n = 2$, the C-section has $z_{oe} = z_{oo}$. This means that the two-port becomes a folded uncoupled section at $f_2 = 2f_1$, which in turns implies that our structure is limited to $n \leq 2$.

III. Implementation, Simulation and Measurement

Fig. 3(a) depicts the layout of the filter with four C-sections on a substrate with $\varepsilon_r = 10.2$ and $\text{thickness} = 1.27$ mm. The perturbation patches A_{p1} and A_{p2} are used to split off the degenerate modes at the two designated frequencies ($f_1 = 2.44$ GHz and $f_2 = 4.49$ GHz). Fig. 3(b) plots the simulated results [12] with $\ell_{c1} = \ell_{c2} = 0$ for testing the electrical length θ_S (evaluated at f_1), where the circuit is weakly coupled by the feed lines. One can see that all $|S_{21}|$ curves possess a dual-resonance response at f_1 and f_2 with two transmission zeros on both the upper and lower sides. Note that only one resonant peak exists and no zero around f_2 when $\theta_S = 90°$, since one of the two degenerate modes has null voltage at the excitation position and it is not activated. Herein, $\theta_S = 60°$ rather than 45° is used since enough space should be saved for ℓ_{c1}.

Table I lists the resonant frequencies when the patches are changed, showing the control of the two bandwidths. The patches are placed at the two symmetric planes of the resonant modes. At f_1, A_{p1} can change the even mode frequency but has no influence on the odd mode, where the voltage is zero. This is exactly the same as the function of the perturbation patch in design of the traditional ring resonator filter [2]. The impact of

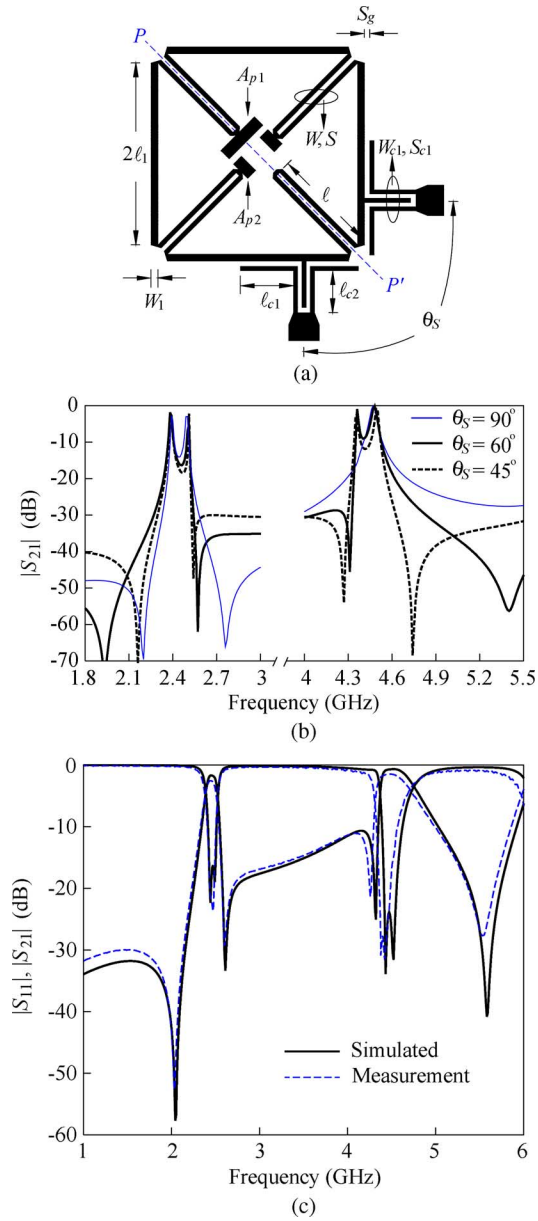

Fig. 3. Filter with four C-sections. (a) Circuit layout. (b) $|S_{21}|$ response with $\ell_{c1} = \ell_{c2} = 0$. (c) Simulated and measured results. Circuit dimensions in mm: $S = 0.164$, $W_1 = 0.25$, $W = W_{c1} = S_{c1} = 0.15$, $S_g = 0.188$, $\ell = 3.81$, $\ell_1 = 3.23$, $\ell_{c1} = 1.57$, $\ell_{c2} = 1.5$. $A_{p1} = 1.7 \times 0.418\ \text{mm}^2$, $A_{p2} = 0.715 \times 0.4\ \text{mm}^2$.

the changes of A_{p2} on the resonance modes at f_1 and f_2 can be explained in a similar way.

The interdigital structure ($\ell_{c1} = 0$) is used to provide coupling from the feed line to the circuit. It is found that the first band needs more coupling to establish the passband. Increasing ℓ_{c1}, however, will decrease the bandwidth at f_2. We had such experience in developing the multi-mode filter in [11]. Then, A_{p2} are increased to compensate this effect. This will decrease the bandwidth at f_1; this in turns contributes a positive factor for establishing a passband with satisfactory return loss. Fig. 3(c) plots the simulated and measured results of the experimental circuit. The fractional bandwidths Δ_1 and Δ_2 at f_1 and f_2 are 3.03% and 6.97%. The measurement shows that the insertion

TABLE I
CONTROL OF TWO BANDWIDTHS WITH A_{P1} AND A_{P2}

A_{p1} (mm^2)	A_{p2} (mm^2)	f_1 (GHz)		f_2 (GHz)	
		even	*odd*	*even*	*odd*
1.2×0.418	0.715×0.4	2.53	2.56	4.53	4.68
1.7×0.418	0.715×0.4	2.50	2.56	4.40	4.68
2.3×0.418	0.715×0.4	2.45	2.56	4.25	4.68
1.7×0.418	0.6×0.4	2.50	2.57	4.44	4.68
1.7×0.418	0.8×0.4	2.50	2.54	4.35	4.68
1.7×0.418	1.0×0.4	2.50	2.5	4.23	4.68

losses are 2.56 dB and 1.45 dB, and return losses 23.5 and 26.4 dB in the first and the second passbands, respectively. The circuit occupies only 27.3% of the area of a traditional ring resonator filter designed at f_1.

Fig. 4(a) plots the layout of the second dual-mode dual-band BPF with six microwave sections, and Fig. 4(b) shows the simulated and measured results. The circuit is designed to have $f_1 = 2.42$ GHz and $f_2 = 4.61$ GHz with $\Delta_1 = 3.5\%$ and $\Delta_2 = 6.24\%$, respectively. At f_1 and f_2, the measured $|S_{21}|$ are 2.39 dB and 1.56 dB, respectively, and the in-band return losses are better than 15 dB. The transmission zeros are at 1.93, 2.57, 4.35, and 5.49 GHz. The circuit has 29.1% of the area of a traditional ring filter. Good agreement between simulated and measured results can be observed.

IV. CONCLUSION

New miniaturized dual-mode dual-band ring resonator BPFs are developed by cascading the microwave C-sections. The circuits use less than one-third of the area of a conventional ring resonator BPF designed at the first frequency. The two experimental circuits demonstrate good inband insertion losses and return losses. In addition, two transmission zeros are created on both sides of each passband. The shortcoming of this circuit structure is the limited tuning range of the second frequency.

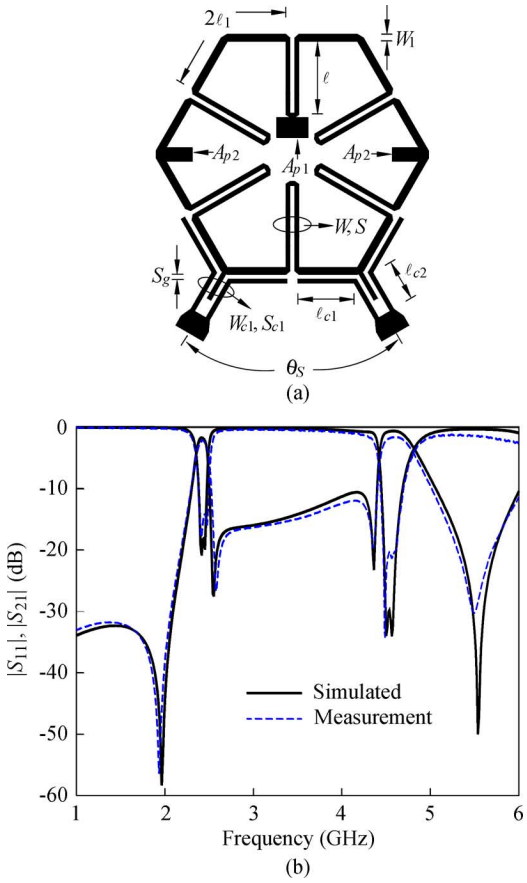

Fig. 4. Dual-mode dual-band BPF with six microwave C-sections. (a) Circuit layout. (b) Simulated and measurement results. Circuit dimensions in mm: $W = 0.148$, $S = 0.157$, $W_1 = 0.25$, $W_{c1} = S_{c1} = S_g = 0.15$, $\ell = 2.51$, $\ell_1 = 2.01$, $\ell_{c1} = 1.94$, $\ell_{c2} = 1.44$. $A_{p1} = 1.1 \times 0.7$ mm^2, $A_{p2} = 0.9 \times 0.47$ mm^2. $\theta_S = 60°$.

REFERENCES

[1] I. Wolff, "Microstrip bandpass filters using degenerate modes of a microstrip ring resonators," *Electron. Lett.*, vol. 8, no. 12, pp. 163–164, Jun. 1972.

[2] A. C. Kundu and I. Awai, "Control of attenuation pole frequency of a dual-mode microstrip ring resonator bandpass filter," *IEEE Trans. Microw. Theory Tech.*, vol. 49, no. 6, pp. 1113–1117, Jun. 2001.

[3] J.-T. Kuo and C.-Y. Tsai, "Periodic stepped-impedance ring resonator (PSIRR) bandpass filter with a miniaturized area and desirable upper stopband characteristics," *IEEE Trans. Microw. Theory Tech.*, vol. 54, no. 3, pp. 1107–1112, Mar. 2006.

[4] J.-X. Chen, T.-Y. Yum, J.-L. Li, and Q. Xue, "Dual-mode dual-band bandpass filter using stacked-loop structure," *IEEE Microw. Wireless Compon. Lett.*, vol. 16, no. 9, pp. 502–504, Sep. 2006.

[5] X. Y. Zhang and Q. Xue, "Novel dual-mode dual-band filters using coplanar-waveguide-fed ring resonators," *IEEE Trans. Microw. Theory Tech.*, vol. 55, no. 10, pp. 2183–2190, Oct. 2007.

[6] A. Görür and C. Karpuz, "Compact dual-band bandpass filters using dual-mode resonators," in *IEEE MTT-S Int. Dig.*, Jun. 2007, pp. 905–908.

[7] C. Lugo and J. Papapolymerou, "Multilayer dual-band filter using a reflector cavity and dual-mode resonators," *IEEE Microw. Wireless Compon. Lett.*, vol. 17, no. 9, pp. 637–639, Sep. 2007.

[8] T.-H. Huang, H.-J. Chen, C.-S. Chang, L.-S. Chen, Y.-H. Wang, and M.-P. Houng, "A novel compact ring dual-mode filter with adjustable second-passband for dual-band applications," *IEEE Microw. Wireless Compon. Lett.*, vol. 16, no. 6, pp. 360–362, Jun. 2006.

[9] B. M. Schiffman, "A new class of broad-band microwave 90-degree phase shifter," *IRE Trans. Microw. Theory Tech.*, vol. 6, no. 6, pp. 232–237, Apr. 1958.

[10] Y.-C. Chiou, J.-T. Kuo, and C.-H. Chan, "New miniaturized dual-band rat-race coupler with microwave C-sections," in *IEEE MTT-S Int. Dig.*, Jun. 2009, pp. 701–704.

[11] Y.-C. Chiou, J.-T. Kuo, and E. Cheng, "Broadband quasi-Chebyshev bandpass filters with multimode stepped-impedance resonators (SIRs)," *IEEE Trans. Microw. Theory Tech.*, vol. 54, no. 8, pp. 3352–3358, Aug. 2006.

[12] IE3D Simulator Zeland Software, Inc., Jan. 1997.